NATURAL CONVECTION INSIDE ECCENTRIC HORIZONTAL ANNULUS FILLED WITH SATURATED POROUS MEDIUM

R.Y. Sakr
Mech. Eng. Dept., Faculty of Eng. (Shoubra), Zagazig University

Abstract

A numerical investigation of natural convection inside eccentric horizontal annulus filled with saturated porous medium is carried out. The solution scheme is based on two-dimensional model, which is governed by Darcy-Oberbeck-Boussinseq equation. The inner cylinder is heated isothermally while the outer one is cooled isothermally.

Discretization of the governing equations is achieved using finite element scheme based on Galerkin method of weighted residuals. The effect of pertinent parameters such as the modified Rayleigh number (Ra) and the relative eccentricity for radius ratio of 2 are considered in this study. The modified Rayleigh number ranges from 10 to 400 while the relative eccentricity (ε) ranges from 0.1 to 0.8. The effect of eccentricity direction is also studied by making runs for eccentricity in horizontal, vertical, 45^o and 315^o orientation.

The numerical results obtained from the present model are compared with the available published results and a good agreement was found. The average Nusselt number and heat transfer as a function of Rayleigh number is presented. Also the flow and heat transfer characteristics are illustrated in terms of stream function and isotherms.

1. Introduction

Natural convection in horizontal porous annuli has a wide variety of technological applications such as insulation of aircraft cabin or horizontal pipes, cryogenics, storage of thermal energy, and underground cable systems. The case considered here, probably of the most practical importance in which the cylinder's surfaces are impermeable and maintained at constant uniform temperatures, with the inner temperature being higher than the outer one. Buoyancy driven flow is induced in the media due to temperature difference.

The case of concentric cylinders has received the most attention in the literature. Caltagirone [1] visualized the isotherms in an annulus of radius ratio of 2, and determined experimentally the Nusselt number based on the temperature measurements of the thermal field. At high Rayleigh numbers, the flow was reported to have a change from two-dimensional to three-dimensional oscillatory motion, partially confirmed by finite element simulation, which let the author to conclude that multi-cellular two-dimensional patterns do not exist. In the same study, the equations governing two-dimensional convection motion were solved using finite difference, but due to the insufficient number of grid points Caltagirone was unable to obtain other flow regimes in addition to the two-cellular one. Echigo et al. [2] also obtained two-dimensional steady state numerical results taking into account the radiation effect.

Burns and Tien [3] examined the variations of the overall heat transfer coefficients with the external heat transfer coefficient and radius ratio by steady-state two-dimensional analyses with the finite difference method and purturbation method. It was indicated that a maximum value of overall heat transfer coefficient existed depending upon the radius ratio. Using finite difference method.

Fukuda et al. [4] obtained three-dimensional results using finite difference method for an inclined annulus. However, the results could not be extended to the horizontal case owing to the

presence of the gravitational force component in the axial direction of the annulus, which is not present in the horizontal case.

Rao el al. [5-6] investigated steady and transient analyses of natural convection in horizontal porous annulus with Galerkin method. They obtained three families of convergent solutions appearing one after the other with increasing modified Rayleigh number corresponding to different initial conditions. They also determined numerically the bifurcation point, which coincide very well with that from the experimental observations of Caltagirone [1].

Two-dimensional numerical work by Mota et al. [7-9] solved two-dimensional Boussinesq equations using finite difference scheme with an ADI method and successive under relaxation to a very fine grid. They showed that for very small radius ratio and on increasing the Rayleigh number, the steady state regime changes from two to four to six to eight cells without exhibiting a hystresis loop. For radius ratio above 1.75 approximately, closed hystersis loops between ranges containing 2 or 4 cells are obtained.

Charrier-Mojtabi et al. [10], observed the two-dimensional two-cellular flow pattern for radius ratio of 2 when Rayleigh number was increased up to 250, after which three-dimensional effect become visible in the upper part of the annulus region. When Rayleigh number decreases the flow pattern become two-dimensional again and consisted of four convection cell flow structures and seems to confirm the hystresis behavior obtained by Mota and Saatdjian [7-9].

Al-fahaid and Sakr [11] studied numerically steady state natural convection in fully saturated porous concentric annuls using Galerkin method. They investigated the effect of modified Rayleigh number and the radius ratio on the Nusselt number at the heated cylinder.

The eccentric annulus was studied numerically by Bau et al., using finite difference and regular perturbation expansion technique [12]. Using a two-term regular perturbation expansion Bau [13] investigated three different geometrical configurations: an eccentric annulus, a buried pipe, and two cylinders one outside the other.

Himasekhar and Bau [14] used boundary layer technique to obtain a correlation for Nusselt number as a function of Rayliegh number and the geometrical parameters valid for a large range of Rayleigh numbers.

Mota and Saatdjian [15] used accurate finite difference code for two-dimensional convection between concentric cylinders and modified it to investigate the flow in eccentric annuli. They used only vertical eccentricity in a range from 0.01 to 0.9 for a radius ratio of 2. They found that the net gain due to eccentricity of insulation could be of order 10% compared with the concentric case. They also, showed that reducing the radius ratio or increasing the eccentricity has the same impact on the geometry in the top part of the layer where the convective effects are more pronounced.

El-Ghanam [16] studied the effect of vertical and horizontal eccentricity in porous horizontal cylindrical annulus for different radius ratios. His results demonstrated that the eccentric insulation is more effective under certain conditions and therefore more economical than the currently used concentric insulation.

Al-fahaid and Sakr [17] studied numerically steady state natural convection in fully saturated porous eccentric horizontal annuls having radius ratio of 2 using Galerkin method. The eccentricity is made on the horizontal axis. The purpose of the present work is to extend the works [16-17] to include the eccentricity in horizontal, vertical, 45^o and 315^o direction and wider range of Rayleigh number.

2. Mathematical Formulation

The model considered here is a porous layer bounded between two horizontal concentric cylinders of radii R_i and R_o as shown in Fig. (1a). The surfaces of the two cylinders are assumed to be maintained at a constant temperatures T_i and T_o respectively with $T_i > T_o$.

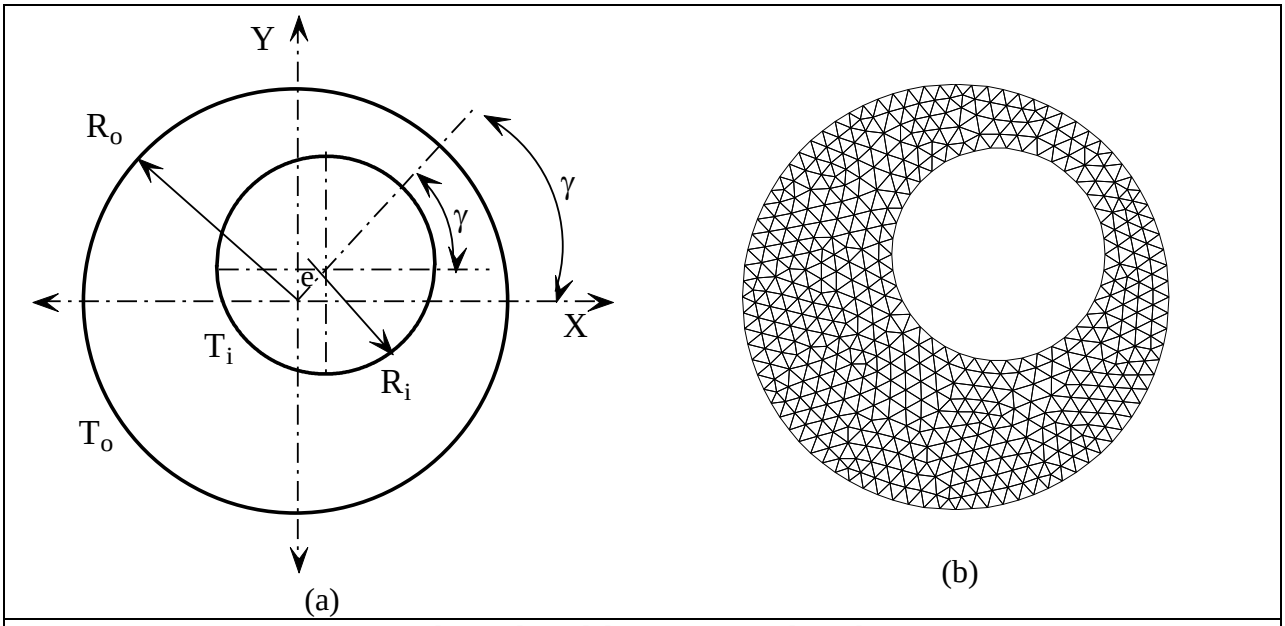

Fig. (1) Physical model geometry and mesh system

2.1 Governing Equations

The governing equations are based on transient natural convection with Boussinesq, Darcy flow, and negligible inertia approximation as follows:

$$\frac{\partial u}{\partial x}+\frac{\partial v}{\partial y}=0 \tag{1}$$

$$\frac{\partial p}{\partial x}+\frac{\mu_f}{K}u=0 \tag{2a}$$

$$\frac{\partial p}{\partial y}+\frac{\mu_f}{K}v-\rho_f g=0 \tag{2b}$$

$$u\frac{\partial T}{\partial x}+v\frac{\partial T}{\partial y}=\frac{k_e}{\rho_f c_f}\left(\frac{\partial^2 T}{\partial x^2}+\frac{\partial^2 T}{\partial y^2}\right) \tag{3}$$

$$\rho_f=\rho_r\left[1-\beta_f(T-T_r)\right] \tag{4}$$

Taking the curl of Eq. (2) and using the approximation of Eq. (4), the following equations are obtained:

$$\nabla^2\psi=-\frac{K}{\mu_f}g\,\rho_r\beta_f\frac{\partial T}{\partial x} \tag{5}$$

$$\nabla^2 T-\frac{\rho_f c_f}{k_e}\left[\frac{\partial\psi}{\partial y}\frac{\partial T}{\partial x}-\frac{\partial\psi}{\partial x}\frac{\partial T}{\partial y}\right]=0 \tag{6}$$

where

$$u=\frac{\partial\psi}{\partial y}\ ,\ v=-\frac{\partial\psi}{\partial x} \tag{7}$$

Introducing the following non-dimensional variables;

$$\theta=\frac{T-T_o}{T_i-T_o}\ ,\quad X=\frac{x}{R_i},\quad Y=\frac{y}{R_i}$$

$$\Psi=\frac{\psi}{\alpha};\ \text{where}\ \ \alpha=\frac{k_e}{\rho_f c_f},$$

The governing equations reduced to:

$$\nabla^2\theta - \left(\frac{\partial\Psi}{\partial Y}\frac{\partial\theta}{\partial X} - \frac{\partial\Psi}{\partial X}\frac{\partial\theta}{\partial Y}\right) = 0 \tag{8}$$

$$\nabla^2\Psi = Ra^* \frac{\partial\theta}{\partial X} \tag{9}$$

where,

Ra^* = Ra. Da

Ra^* is the modified Rayleigh number and is given by: $Ra^* = g\rho_f \rho_r c_f \beta_f K(T_i - T_o)R_i / k_e\mu_f$

Ra; is Rayleigh number and given by:

$Ra = g\rho_f \rho_r c_f \beta_f (T_i - T_o)R_i^3 / k_e\mu_f$

Da; is Darcy number and given by:

$Da = K / R_i^2$

2.2 Boundary Conditions

The boundary conditions are handled as follows:-

a- at the inner cylinder surface

$$\Psi = 0, \quad \theta = 1.0 \tag{10a}$$

b- at the outer cylinder surface

$$\Psi = 0, \quad \theta = 0 \tag{10b}$$

2.3 Heat Transfer Calculations

The local Nusselt number at the inner and outer cylinders surfaces can be calculated from the following equations respectively:

$$Nu_i = \frac{\bar{h} R_i}{\lambda_e} = -\left(\frac{\partial\theta}{\partial n}\right)_{X^2+Y^2=R_i} \tag{11a}$$

$$Nu_o = -\left(\frac{\partial\theta}{\partial n}\right)_{X^2+Y^2=R_o} \tag{11b}$$

where n: represent the direction normal to the cylinder surface.

The steady state average Nusselt number at the inner or outer cylinders surfaces are as given by:

$$\overline{Nu}_i = \frac{1}{2\pi}\int_0^{2\pi} Nu_i(\gamma)\, d\gamma \tag{12a}$$

$$\overline{Nu}_o = \frac{1}{2\pi}\int_0^{2\pi} Nu_o(\gamma)\, d\gamma \tag{12b}$$

3. Numerical Solution

The solutions of Eqs. (8) and (9) with the boundary conditions specified by Eq. (10) are obtained numerically by using the Galerkin based finite element method [17, 19]. The finite element technique is used to reduce the system of governing equations into a discretized set of

algebraic equations. The procedure begins with the division of the continuum region of interest into a number of simply shaped regions called elements. The grid system used in the present calculation is illustrated in Fig. (1b). The element type which used here is linear triangular element. The approximate expressions of temperature and stream function in an element are given by polynomials in terms of the nodal values and interpolation functions. The interpolation functions are derived from the assumption of linear variation of temperature and stream function through the element and are given by the following equation:

$$\psi^e = \sum_{m=1}^{3} N_m \Psi_m \tag{13a}$$

$$\theta^e = \sum_{m=1}^{3} N_m \theta_m \tag{13b}$$

where,

N_m is the usual interpolation function and is defined by:

$$N_m = \frac{1}{2A}\,(a_m + b_m X + c_m Y) \tag{14}$$

where,

A is the element area and

$$\begin{aligned} a_1 &= X_2 Y_3 - X_3 Y_2 \\ b_1 &= Y_2 - Y_3 \\ c_1 &= X_3 - X_2 \end{aligned} \tag{15}$$

The other components are given by cyclic permutation of the subscripts in the order 1,2 and 3. If the approximations given by Eq. (13) are substituted in the governing Eqs.(8-9), and the global errors are minimized using the above interpolation functions N_i as weighting functions. After performing the weighted integration over the domain G and the application of Green's theorem, The present model is converted into:

$$[K_1]\,\{\theta\} = \{F_1\} \tag{16a}$$

$$[K_2]\,\{\Psi\} = \{F_2\} \tag{16b}$$

where,

$$[K_1] = \sum_{e=1}^{E} \int_{\Omega^e} \left(\frac{\partial [N]^T}{\partial X}\cdot\frac{\partial [N]}{\partial X} + \frac{\partial [N]^T}{\partial Y}\cdot\frac{\partial [N]}{\partial Y}\right) d\Omega^e$$

$$+ \sum_{e=1}^{E} \int_{\Omega^e} \left(\Psi_Y [N]^T \cdot \frac{\partial [N]}{\partial X} - \Psi_X [N]^T \cdot \frac{\partial [N]}{\partial Y}\right) d\Omega^e$$

$$\{F_1\} = \sum_{e=1}^{E} \int_{\Gamma^e} \left([N]^T \frac{\partial N}{\partial X} + [N]^T \frac{\partial N}{\partial Y}\right) d\Gamma^e$$

$$[K_2] = \sum_{e=1}^{E} \int_{\Omega^e} \left(\frac{\partial [N]^T}{\partial X}\cdot\frac{\partial [N]}{\partial X} + \frac{\partial [N]^T}{\partial Y}\cdot\frac{\partial [N]}{\partial Y}\right) d\Omega^e$$

$$\{F_2\} = \sum_{e=1}^{E} \int_{\Gamma^e} [N]^T \frac{\partial [N]}{\partial X} d\Gamma^e + \int_{\Gamma^e} [N]^T \frac{\partial [N]}{\partial Y} d\Gamma^e + \sum_{e=1}^{E} \int_{\Omega^e} Ra\,\theta [N]^T \frac{\partial [N]}{\partial X} d\Omega^e$$

and

E = total number of elements, Ω bounded domain, Γ domain boundary,

$$\Psi_Y = \frac{\partial \Psi}{\partial Y}, \quad \Psi_X = \frac{\partial \Psi}{\partial X},$$

Equations (8) and (9) result in two systems of linear equations. Equation (16a, b), that are solved iteratively by Gauss elemination method through a FORTRAN computer code. The iterative procedure is terminated when the following relative convergence criterion is satisfied:

$$\left|\frac{\Psi^{i+1} - \Psi^{i}}{\Psi^{i+1}}\right| \leq 10^{-4}$$

where, i denotes the iteration number performed.

4. Model Validation

First the present numerical method is validated by solving the traditional convection problem for two concentric horizontal cylinders. The obtained results are compared with the available published data. Table 1 shows the average Nusselt Number for previous researchers. In comparison with the present results good agreement is found.

Table 1: Comparison of the average Nusselt number for natural convection flow in porous medium between two concentric cylinders with radius ratio of 2.

	Caltagirone [1]	Rao et al. [3]	Bau [12]	Facas [20]	Facas & Farouk [21]	Present result
Grid size	49x49	10x10	30x44	50x50	25x25	10x18
Ra=50	1.328	1.341	1.335	1.342	1.362	1.317
Ra=100	1.829	1.861	1.844	1.835	1.902	1.865

5. Results and Discussions

The average Nusselt number at the inner hot cylinder as a function of the relative eccentricity in the horizontal direction is depicted in Fig. (2), at different Rayleigh numbers for a range of relative eccentricity from 0.1 to 0.8. It is shown that, as Rayleigh number increases the average Nusselt number increases and the curves have a minimum values located at zero eccentricities. This indicates that the concentric insulation is preferable than the eccentric one. For higher values of Rayleigh numbers the total heat flow can be reduced by eccentric insulation. The values of relative eccentricity that locates the minimum heat flow rate increases with the increase of Rayleigh number.

The average Nusselt number at the inner hot cylinder as a function of the relative eccentricity in the vertical direction is depicted in Fig. (3), for different Rayleigh number. For higher values of Rayleigh numbers the average Nusselt number can be reduced or increased according to the value of the relative eccentricity.

The average Nusselt number at the inner hot cylinder as a function of the relative eccentricity in the 45^{o} to the horizontal direction is depicted in Fig. (4), at different Rayleigh numbers. It is shown from the figure that as either Rayleigh number or at the relative eccentricity increase the average Nusselt number increases.

The average Nusselt number at the inner hot cylinder as a function of the relative eccentricity in the 315^{o} to the horizontal direction is depicted in Fig. (5), for different Rayleigh number. The increase of relative eccentricity and Rayleigh number lead to an increase in the average Nusselt number.

Figure (6) shows the stream functions for a relative eccentricity of 0.2 in the horizontal direction at different Rayleigh numbers of 10, 160, and 300 respectively. It is shown from the figure that the flow is composed of two unsymmetrical cells and the centers of cells rise upward as Rayleigh number increases. Also, it is depicted from the figure that the intensity of the

contour lines increases near the walls of the inner and outer cylinders. Also, the values of stream function in both cells are different and opposite in signs depends on the flow direction. Figure (7) illustrates the corresponding isotherms. It is shown from the figure that, the isotherms are nearly circular at Ra=10. So, the conduction is the dominant mode of heat transfer and as the Rayleigh number increases the convection becomes dominant and it is noted that the intensity of isotherms become larger at the bottom of the inner cylinder and at the top of the outer cylinder, indicating more heat transfer rate at these location.

Figure (8) shows the contour lines of stream function for relative eccentricity in the horizontal direction of having a value of 0.5 and different Rayleigh numbers having values of 10, 160 and 300 respectively. The flow patterns are composed of two unsymmetrical flow cells. In all cases the centers of cells moves upward and becomes bigger as Rayleigh number increases. The corresponding isotherms are illustrated in Fig. (9), from the figure, it is clear that the conduction is the dominant mode of heat transfer of heat transfer at Ra=10. As Rayleigh number increases the convection plays its role in the heat transfer process. More intensive isotherms at the bottom of inner cylinder and at the top of the outer cylinder.

The same behavior of the flow and heat transfer characteristics for relative eccentricity in the horizontal direction having a value of 0.7 and Rayleigh number having values of 10, 160 , and 300 are illustrated in Figs. (10-11) respectively.

For all cases, it is noticed that separation of the thermal boundary layer takes place as Rayleigh number increases and larger stratification, which is denoted by the straight line portions of the isotherms in the wider portion of the annulus takes place.

Figure (12) illustrates the contour lines of stream function for relative eccentricity in the vertical direction is having a value of 0.2 and different Rayleigh numbers having values of 10, 160, and 300 respectively. It is shown from the figure that the flow is composed of two symmetrical cells about the vertical axis and the centers of cells rise upward as Rayleigh number increases. Figure (13) shows the corresponding isotherms. It is shown from the figure that, the isotherms are nearly circular at Ra=10. So, the conduction is the dominant mode of heat transfer and as the Rayleigh number increases the convection becomes dominant and it is noted that the intensity of isotherms become larger at the bottom of the inner cylinder and at the top of the outer cylinder, indicating more heat transfer rate at these location.

The contour lines of stream function for relative eccentricity in the vertical direction having a value of 0.5 and different Rayleigh numbers having values of 10, 160 and 300 respectively is shown in Fig. (14). It is shown from the figure that, the flow pattern is composed of two flow cells at Ra=10 and four flow cells for Ra=160 and 300 respectively. The corresponding isotherms are illustrated in Fig. (15), from the figure, it is clear that the conduction is the dominant mode of heat transfer of heat transfer at Ra=10. As Rayleigh number increases the convection plays its role in the heat transfer process. More intensive isotherms at the bottom of inner cylinder and at the top of the outer cylinder. The same behavior of the flow and heat transfer characteristics for relative eccentricity in the vertical direction having a value of 0.7 and Rayleigh number having values of 10, 160 , and 300 are illustrated in Figs. (16-17) respectively.

Figure (18) shows the contour lines of stream function for relative eccentricity in the 45^{o} to the horizontal direction having a value of 0.2 and different Rayleigh numbers having values of 10, 120, and 300 respectively. It is shown from the figure that, the flow is composed of two unsymmetrical cells and the centers of cells rise upward and become bigger as Rayleigh number increases and having different values. The corresponding isotherms are illustrated in Fig. (19).

The contour lines of stream function for relative eccentricity in the 45^{o} to the horizontal direction having a value of 0.4 and different Rayleigh numbers having values of 10, 80, and 120 respectively are shown in Fig. (20). It is shown from the figure that, the flow is composed of two

unsymmetrical cells and the centers of cells rise upward and become bigger as Rayleigh number increases having different values. The corresponding isotherms are illustrated in Fig. (21).

Figure (22) shows the contour lines of stream function for relative eccentricity in the 45^o to the horizontal direction having a value of 0.6 and different Rayleigh numbers are having values of 10, 80, and 120 respectively. It is shown from the figure that the flow is composed of two unsymmetrical cells and the centers of cells rise upward and become bigger as Rayleigh number increases having different values. The corresponding isotherms are illustrated in Fig. (23).

Figure (24) shows the contour lines of stream function for relative eccentricity in the 315^o to the horizontal direction having a value of 0.2 and different Rayleigh numbers having values of 10, 200, and 300 respectively. It is shown from the figure that the flow is composed of two unsymmetrical cells and the centers of cells rise upward and become bigger as Rayleigh number increases having different values. The corresponding isotherms are illustrated in Fig. (25). The separation of the thermal boundary layer is depicted as Rayleigh number increases.

Figure (26) shows the contour lines of stream function for relative eccentricity in the 315^o to the horizontal direction having a value of 0.4 and different Rayleigh numbers having values of 10, 200, and 300 respectively. It is shown from the figure that the flow is composed of two unsymmetrical cells and the centers of cells rise upward and become bigger as Rayleigh number increases having different values. The corresponding isotherms are illustrated in Fig. (27).

Figure (28) shows the contour lines of stream function for relative eccentricity in the 315^o to the horizontal direction having a value of 0.2 and different Rayleigh numbers having values of 10, 200, and 300 respectively. It is shown from the figure that the flow is composed of two unsymmetrical cells and the centers of cells rise upward and become bigger as Rayleigh number increases having different values. The corresponding isotherms are illustrated in Fig. (29).

6. Conclusions

The numerical investigation of natural convection inside eccentric annulus filled with saturated porous medium for radius ratio of 2 is carried out. The followings are the main points that can be concluded from the present study:-

1. An accurate finite element code was developed to solve the two-dimensional Darcy-Boussinesq equations for an eccentric horizontal annulus filled with saturated porous medium and the eccentricity was made in different directions.
2. For $Ra \leq 10$, the concentric insulation is the most efficient as the average Nusselt number has a minimum at zero relative eccentricity.
3. For eccentricity in any direction the average Nusselt number is increased by the increase of Rayleigh number.
4. For higher values of Rayleigh number, the average Nusselt number a has minimum or maximum at different relative eccentricity according to the eccentricity direction and the value of Rayleigh number.
5. Except for the direction 45^o to the horizontal, the present code is able to predict the present phenomenon for Rayleigh number up to 400 and any acceptable value of relative eccentricity.
6. Generally, the effect of Rayleigh number on the average Nusselt number is more significant than the effect of relative eccentricity except for abrupt change conditions.

Nomenclature

A element area
c specific heat
Da Darcy number, $Da=K/R_i^2$
e eccentricity
E total number of elements
{F} force vector
g gravity vector
G bounded domain
h heat transfer coefficient
K permeability
[K] stiffness matrix
k_e effective thermal conductivity of the porous media
Nu Nusselt number
n normal direction
N interpolation function
R radius ratio, Ro/Ri
Ri inner cylinder radius
R_o outer cylinder radius
Ra Rayleigh number, $Ra = g\rho_f \rho_r c_f \beta_f (T_i - T_o)R_i^3 / k_e\mu_f$
Ra* modified Rayleigh number, $Ra^* = g\rho_f \rho_r c_f \beta_f K(T_i - T_o)R_i / k_e\mu_f$
T temperature
u velocity component in x-direction
v velocity component in y-direction
x, y Cartesian coordinates
X, Y dimensionless Cartesian coordinates

Greek

α thermal diffusivity of the porous medium
β thermal expansion coefficient
γ circumferential angle
Γ domain boundary
θ dimensionless temperature
μ viscosity
ρ density
ψ stream function
Ψ dimensionless stream function
ε relative eccentricity = e/R_i

Subscripts

e effective
f fluid
i. inner
o outer
r. reference
x,y Cartesian components

Superscripts

e. element level
i. iteration number
T transpose
– average

References:

1. Caltagirone, J.P., 1976, "Thermo-Convective Instability in Porous Medium Bounded By Two Concentric Horizontal Cylinders," J. of Fluid Mechanics, Vol. 76, pp. 337-362.
2. Echigo, R., Hasegawa, S. Tottori, S., Shimonure, H. and Okamoto, Y., 1978, "An Analysis on the Radiation and Free Convective Heat Transfer in Horizontal Annulus with Permeable Insulators," Proc. 6 th International Heat Transfer Conf., Vol. 3, pp. 385-390.
3. Burns, P.J. and Tien, C.L., "Natural Convection in Porous Media Bounded by Concentric Spheres and Horizontal Cylinders," Int. J. of Heat Mass Transfer, Vol. 22, pp. 929-939.

4. Fukuda, K., Takuka, Y. and Hasegawa, S., "Three-dimensional Natural Convection in a Porous Medium between Concentric Inclined Cylinders", Vol. HTD-8, 1981, ASME, Orlando, FL., pp. 97-103.
5. Rao, Y.F., Fukuda, K. and Hasegawa, S., "Steady and Transient Analysis of Natural Convection in a Horizontal Porous Annulus with Galerkin Method," ASME J. of Heat Transfer, Vol. 109, 1987, pp. 919-927.
6. Rao, Y.F., Fukuda, K. and Hasegawa, S., "A Numerical Study of Three-Dimensional Natural Convection in a Horizontal Porous Annulus with Galerkin Method," Int. J. Heat Mass Transfer, Vol. 31, 1989, pp. 695-707.
7. Mota, J.P.B., and Sattdjian, F., "Natural Convection in Porous Horizontal Cylindrical Annulus," ASME J. of Heat Transfer, Vol. 116, 1994, pp. 621-626.
8. Mota, J.P.B., and Sattdjian, F., "Natural Convection in Porous Cylindrical Annuli ", Int. J. Num. Methods Heat Fluid Flow, Vol. 5, 1995, pp. 3-12.
9. Mota, J.P.B., and Sattdjian, F., "On the Reduction of Natural Convection Heat Transfer in Horizontal Eccentric Annuli Containing Saturated Porous Media," Int. J. Num. Methods Heat Fluid Flow, 7 (4), pp. 401-416, 1997.
10. Carrier-Mojtabi, M.C., Mojtabi, A. Azaiez, M. and Labrosse, G., "Numerical and Experimental Study of multi-cellular Free Convection Flows in an Annular porous Layer", Int. J. Heat Mass Transfer, Vol. 34, 1991, pp. 3061-3074.
11. Al-Fahaid, A.F. and Sakr, R.Y., "Numerical Study of Natural Convection Heat Transfer in Horizontal Annuli Containing Saturated Porous media", Second Saudi Technical Conference and Exhibition STCEX 2002, Vol. 3, pp. 68-76.
12. Bau, H.H. "Thermal Convection in a Horizontal, Eccentric Annulus Containing a Saturated Porous Medium- An Extended Purturbation Expansion", Int. J. Heat Mass Transfer, Vol. 27, pp. 2277-2287, 1984.
13. Bau, H.H., 1984, "Low Rayleigh Number Thermal Convection in Saturated Porous Medium Bounded by Two Horizontal Eccentric Cylinders," ASME J. of Heat Transfer, Vol. 106, 1984, pp. 166-175.
14. Himasekhar, K. and Bau, H. H., "Large Rayleigh Number Convection in a Horizontal Eccentric Annulus Containig Saturated Porous Media", Int. J. Heat Mass Transfer, Vol. 29, 1986, pp. 703-12.
15. Mota, J.P.B., and Sattdjian, F., "Natural Convection in Porous Horizontal Cylindrical Annulus," ASME J. of Heat Transfer, Vol. 116, 1994, pp. 621-626.
16. El-Ghanam, R.I, " Effect of Vertical and Horizontal Eccentricity on Natrual Convection in a Porous Horizontal Cylindrical Annulus", Engng. Res. Jour., Vol. 60, pp.99-114, December 1998, Helwan University.
17. Al-Fahaid, A.F. and Sakr, R.Y., "Numerical Investigation of Natural Convection Inside Eccentric Horizontal annulus Filled with Saturated Porous Media, Part I – Horizontal Eccentricity, HEFAT 2004.
18. Rao, S. S., The Finite Element Methods in Engineering, Pergamon Press, 1982.
19. Pepper, D.W., and Heinrich, J.C., The Finite Element Method- Basic Concepts and Applications, Hemisphere Publishing Corporation, 1992.
20. Facas, G.N., "Natural Convection From a Buried Pipe with External Baffles", Numerical Heat Transfer, Part A, 27:595-609, 1995.
21. Facas, G.N and Farouk, B. "Transient and Steady State Natural Convection in a Porous Medium between Two Concentric Cylinders", ASME J. Heat Transfer, Vol. 105, pp. 660-663, 1983.

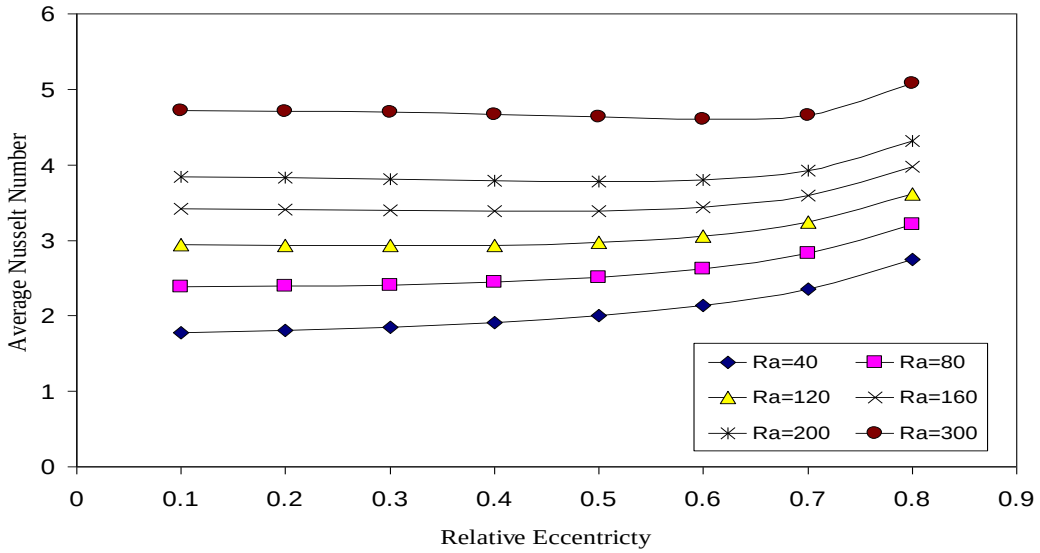

Fig. (2) Variation of the average Nusselt number with relative eccentricity for different Rayleigh numbers (eccentricity in horizontal direction)

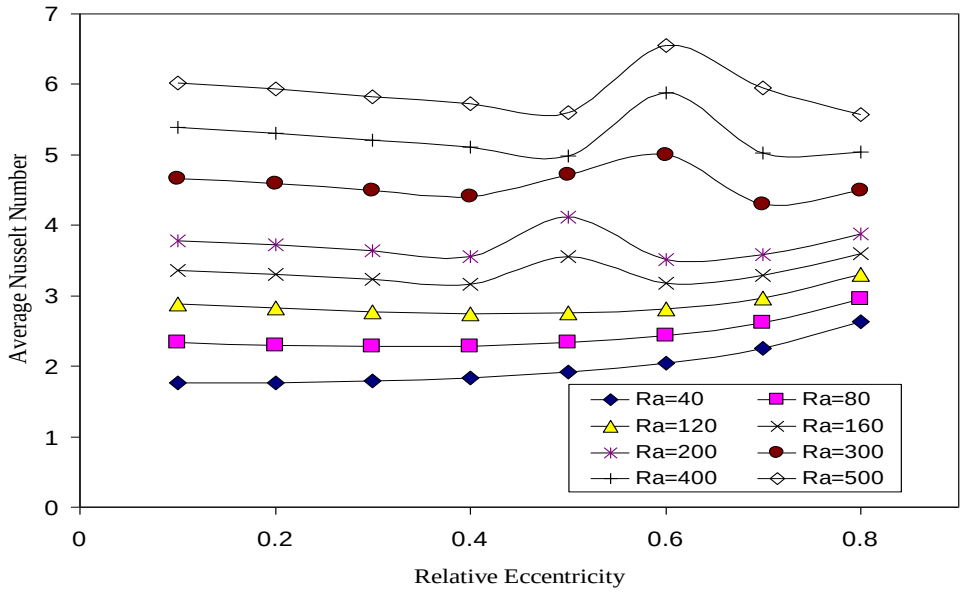

Fig. (3) Variation of the average Nusselt number with relative eccentricity for different Rayleigh numbers (eccentricity in vertical direction)

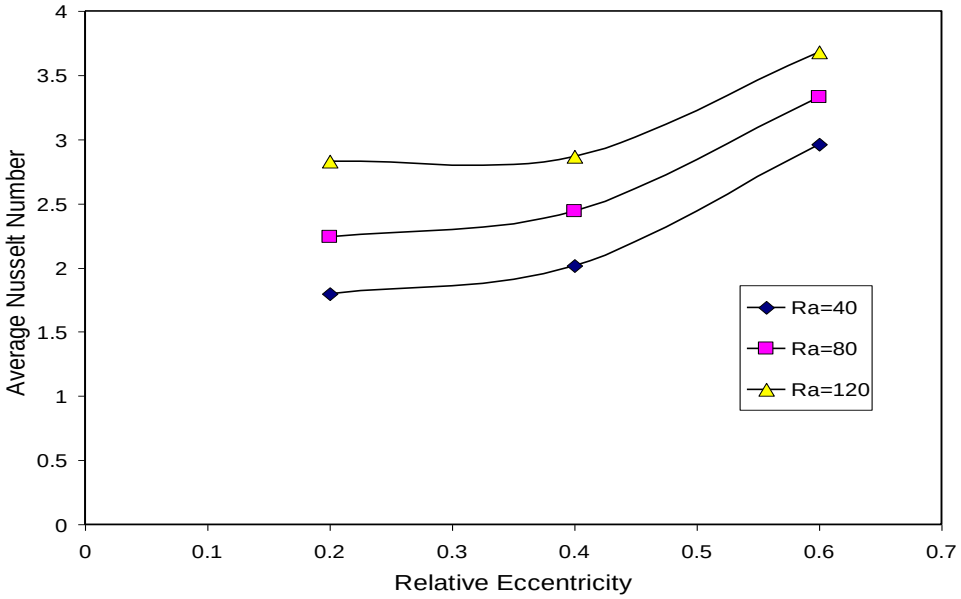

Fig. (4) Variation of the average Nusselt number with relative eccentricity for different Rayleigh numbers (eccentricity in 45^{o} direction)

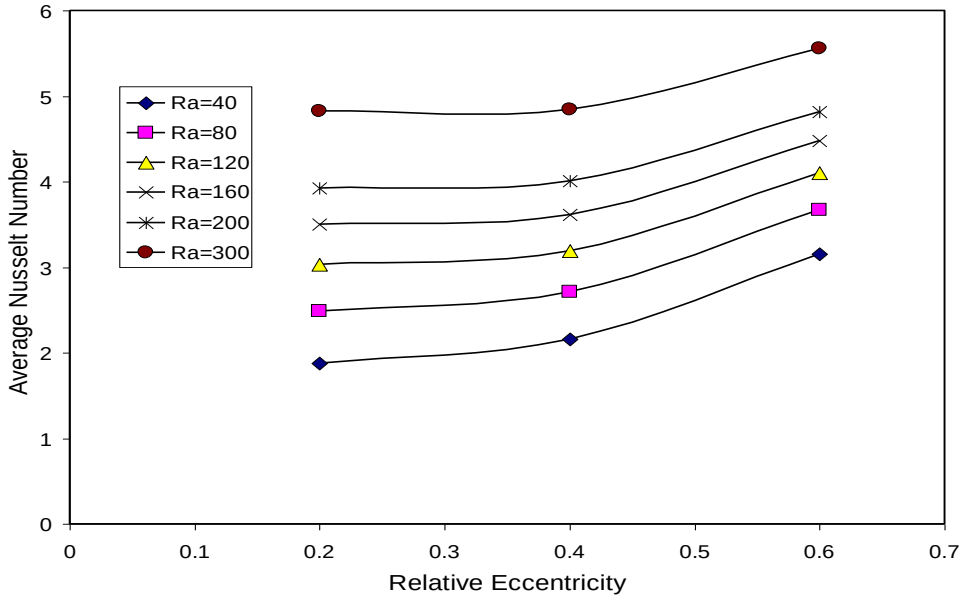

Fig. (5) Variation of the average Nusselt number with relative eccentricity for different Rayleigh numbers (eccentricity in 315^{o} direction)

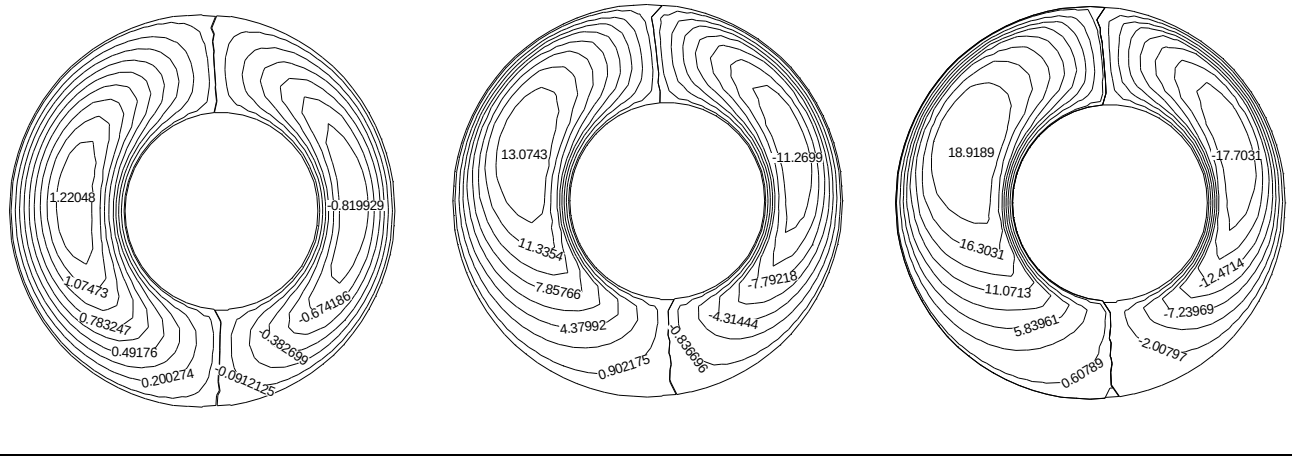

Fig. (6) Stream function contours for relative eccentricity of 0.2 and Rayleigh number of 10, 160 and 300 respectively, (eccentricity in horizontal direction)

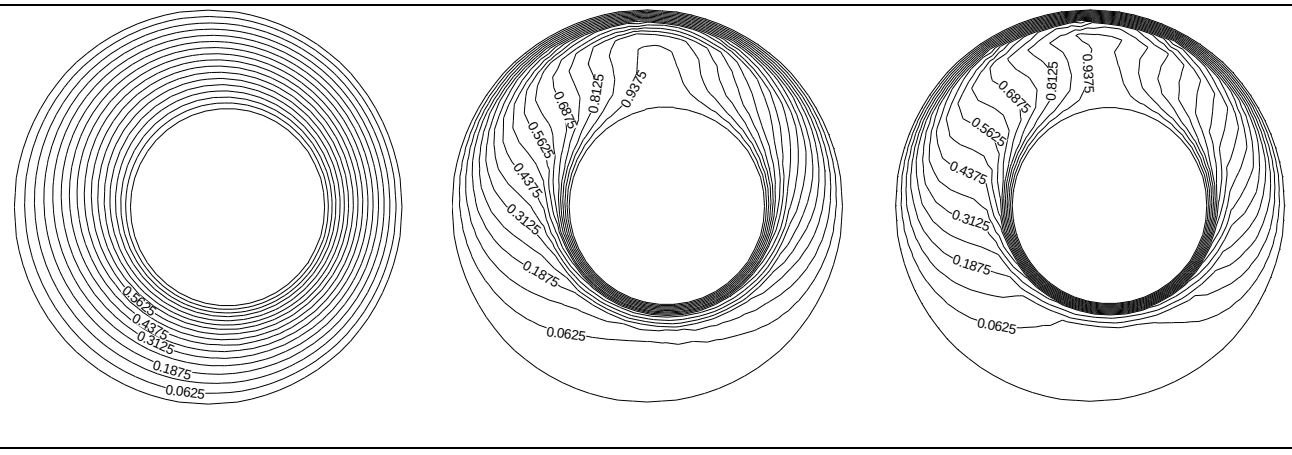

Fig. (7) Isotherms contours for relative eccentricity of 0.2 and Rayleigh number of 10, 160 and 300 respectively, (eccentricity in horizontal direction)

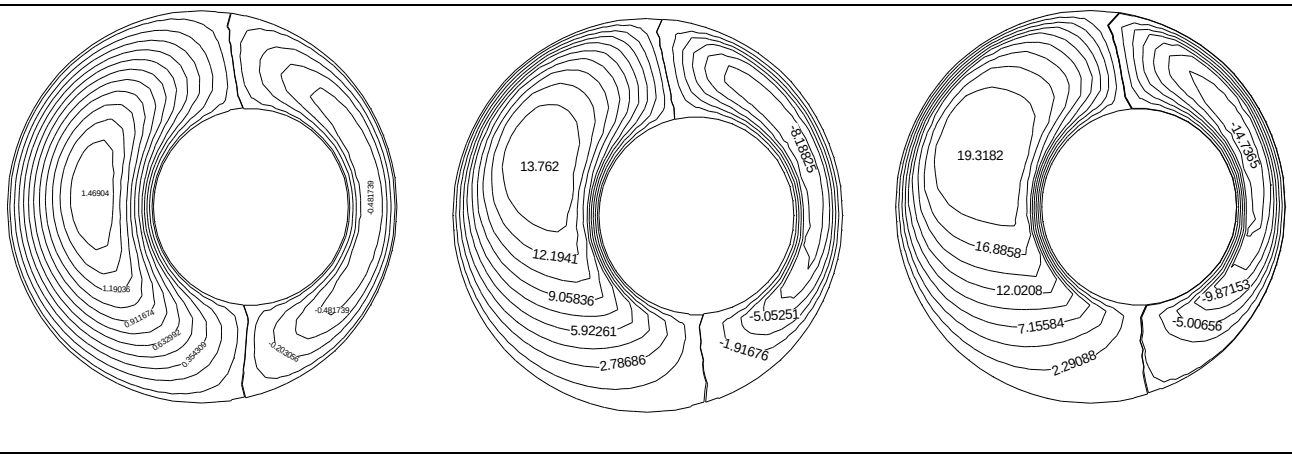

Fig. (8) Stream function contours for relative eccentricity of 0.5 and Rayleigh number of 10, 160 and 300 respectively, (eccentricity in horizontal direction)

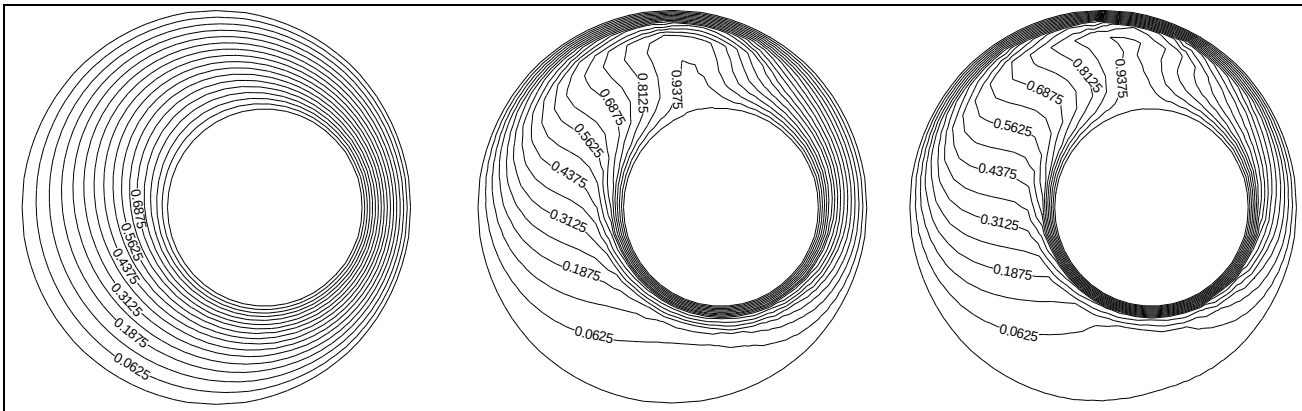

Fig. (9) Isotherms contours for relative eccentricity of 0.5 and Rayleigh number of 10, 100 and 300 respectively, (eccentricity in horizontal direction)

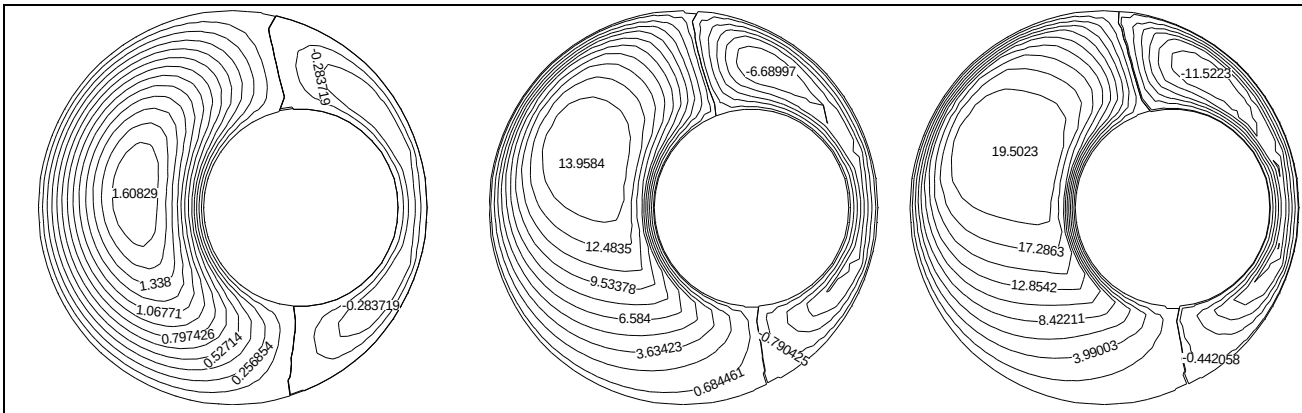

Fig. (10) Stream function contours for relative eccentricity of 0.7 and Rayleigh number of 10, 160 and 300 respectively, (eccentricity in horizontal direction)

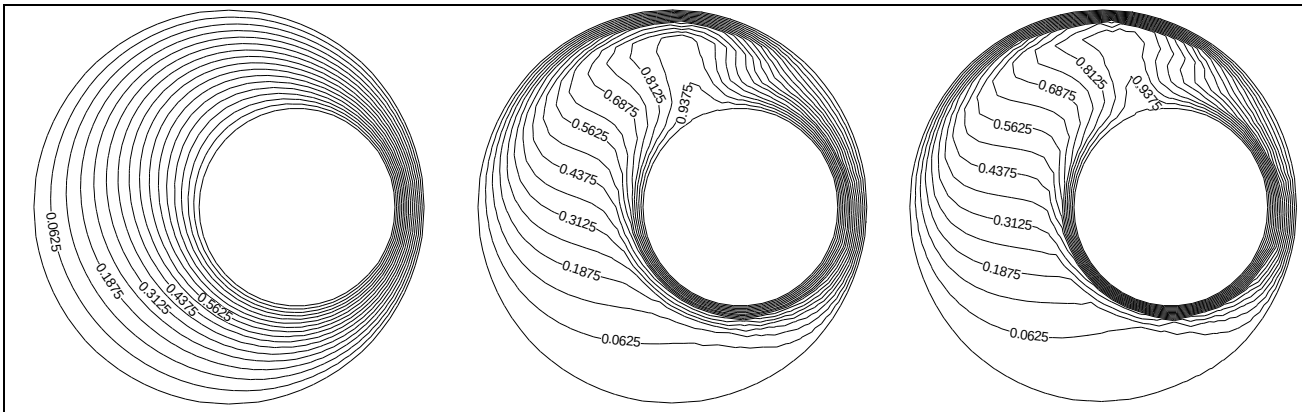

Fig. (11) Isotherms contours for relative eccentricity of 0.7 and Rayleigh number of 10, 160 and 300 respectively, (eccentricity in horizontal direction)

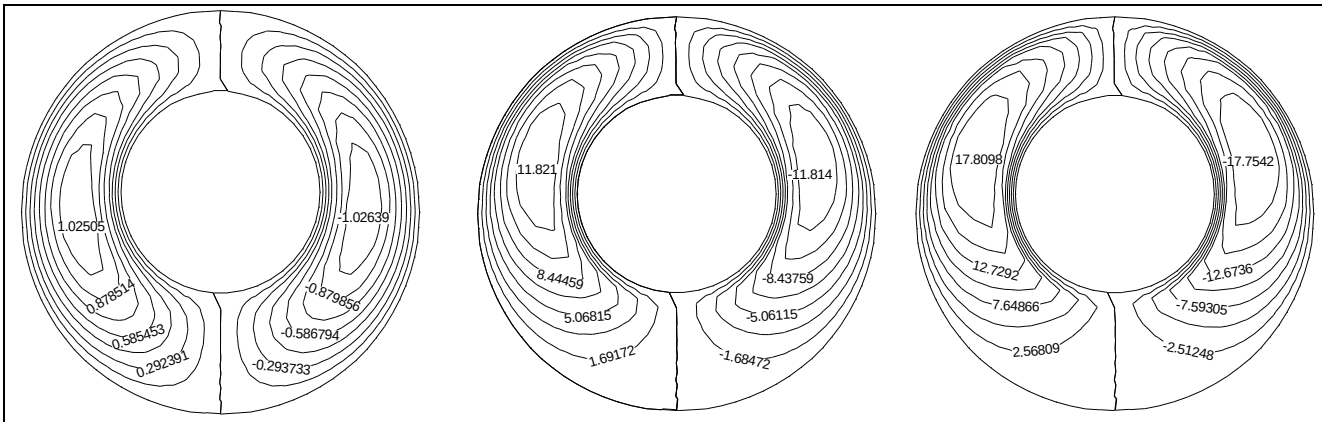

Fig. (12) Stream function contours for relative eccentricity of 0.2 and Rayleigh number of 10, 160 and 300 respectively, (eccentricity in vertical direction)

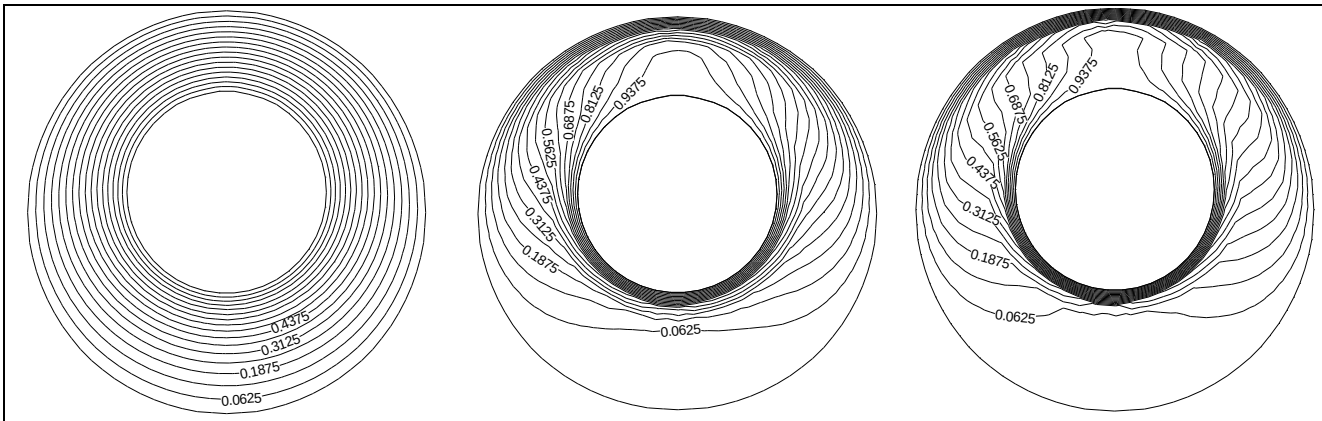

Fig. (13) Isotherms contours for relative eccentricity of 0.2 and Rayleigh number of 10, 160 and 300 respectively, (eccentricity in vertical direction)

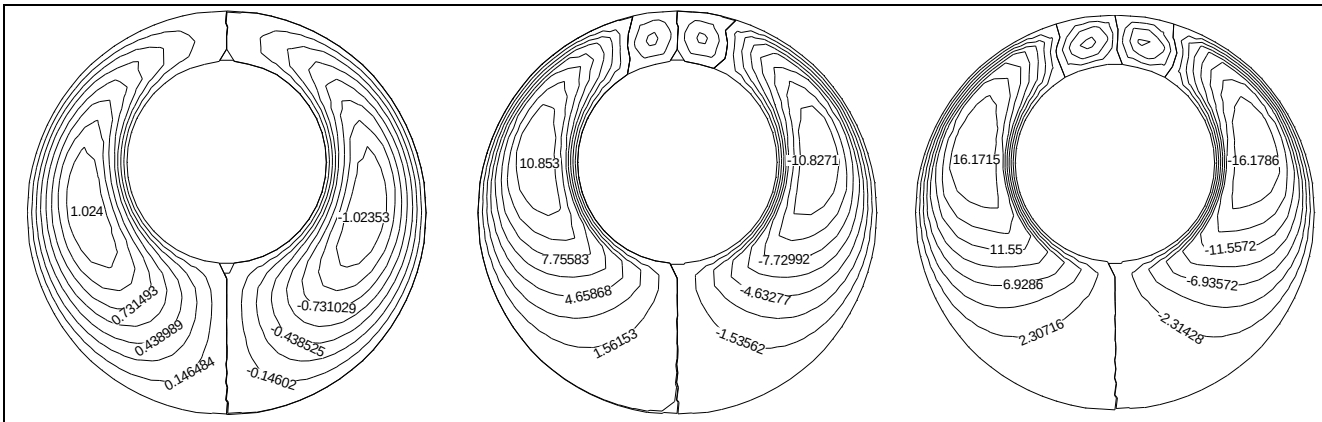

Fig. (14) Stream function contours for relative eccentricity of 0.5 and Rayleigh number of 10, 160 and 300 respectively, (eccentricity in vertical direction)

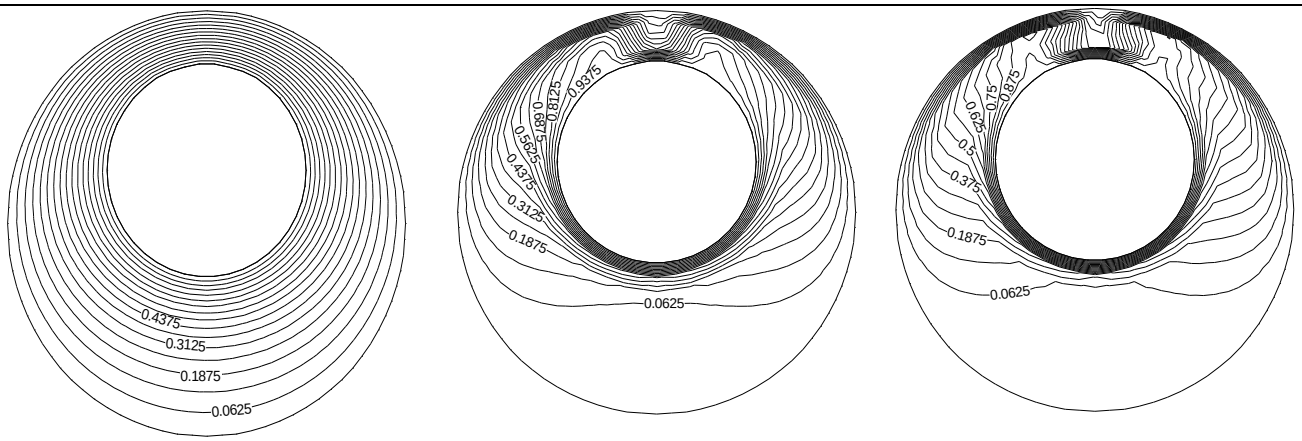

Fig. (15) Isotherms contours for relative eccentricity of 0.5 and Rayleigh number of 10, 160 and 300 respectively, (eccentricity in vertical direction)

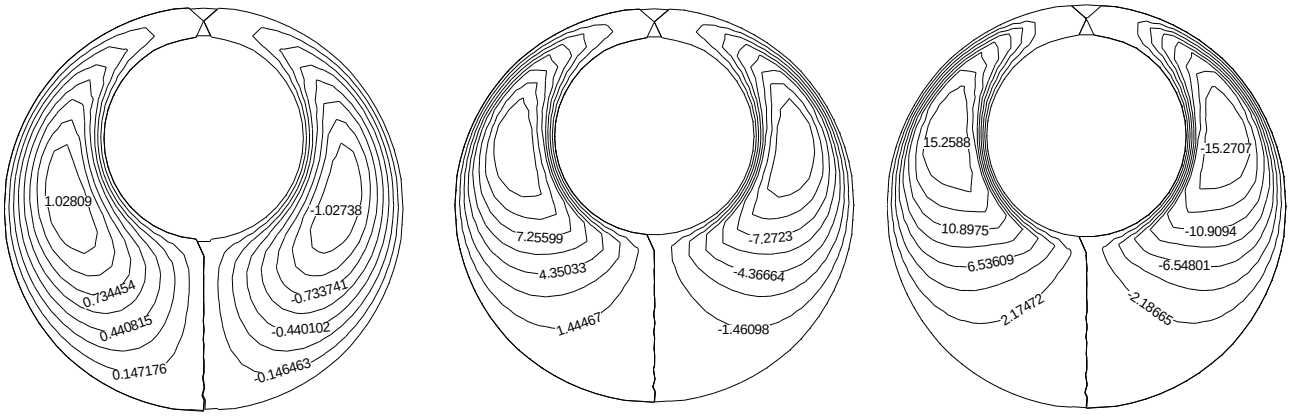

Fig. (16) Stream function contours for relative eccentricity of 0.7 and Rayleigh number of 10, 160 and 300 respectively, (eccentricity in vertical direction)

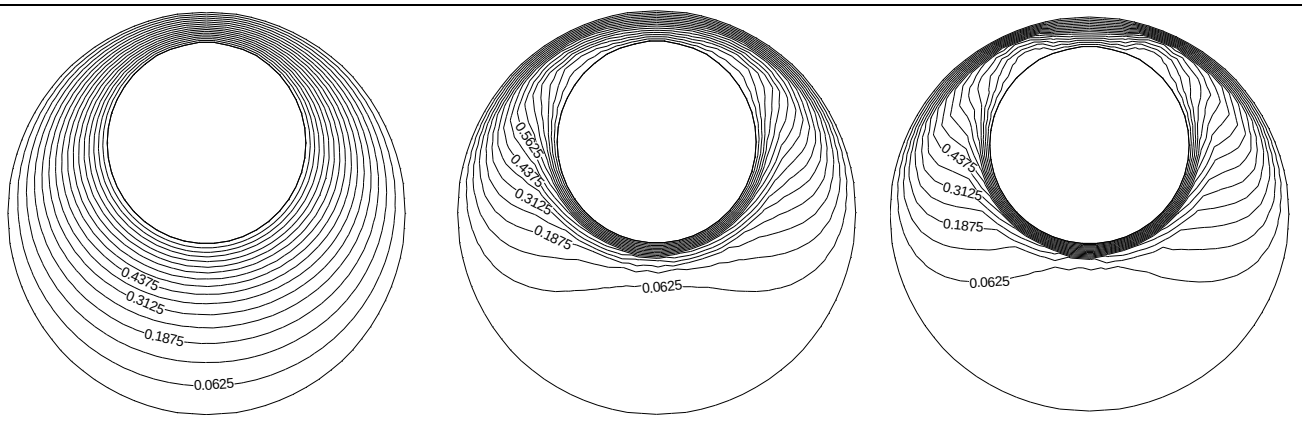

Fig. (17) Isotherms contours for relative eccentricity of 0.7 and Rayleigh number of 10, 160 and 300 respectively, (eccentricity in vertical direction)

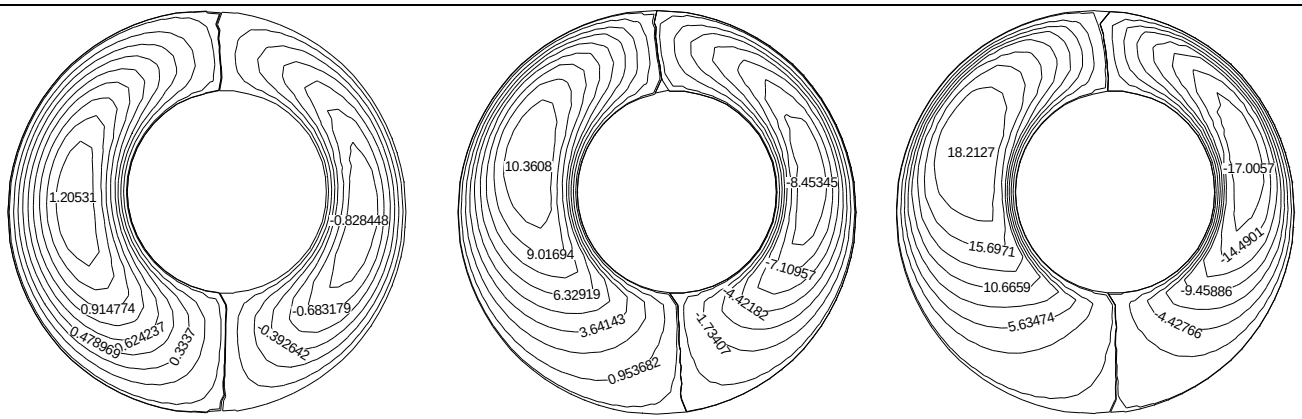

Fig. (18) Stream function contours for relative eccentricity of 0.2 in direction 45^{o} to the horizontal and Rayleigh number of 10, 120 and 300 respectively

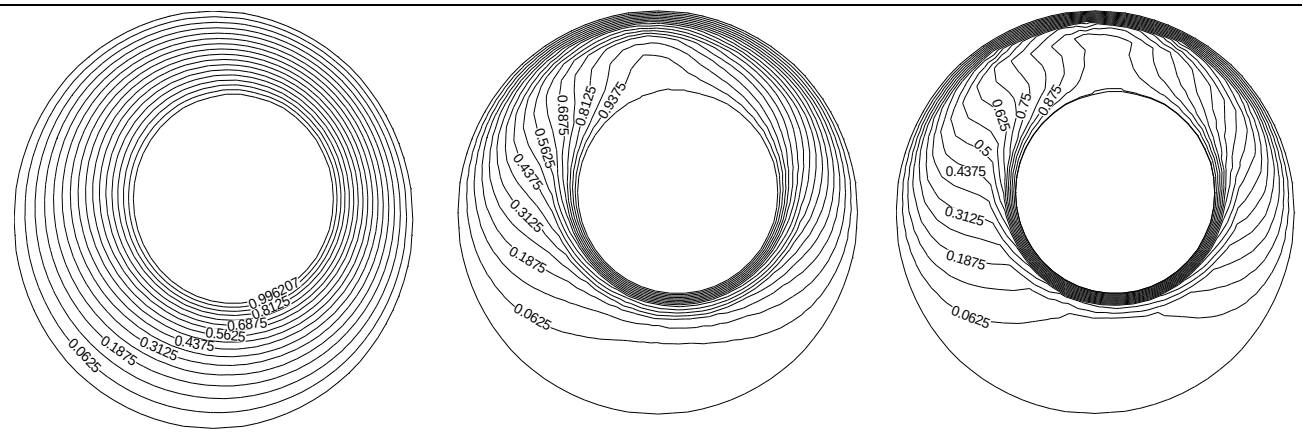

Fig. (19) Isotherms contours for relative eccentricity of 0.2 in direction 45^{o} to the horizontal and Rayleigh number of 10, 120 and 300 respectively

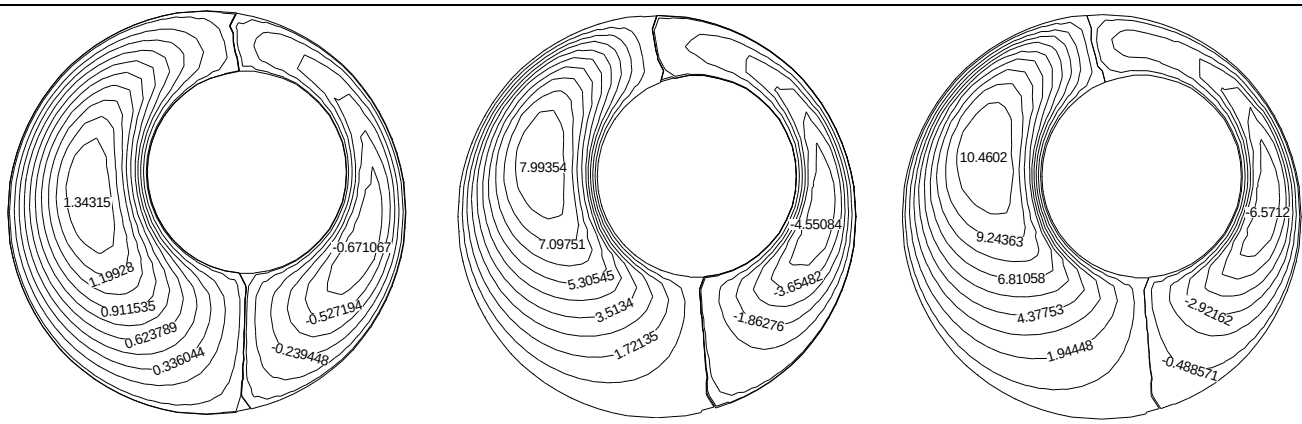

Fig. (20) Stream function contours for relative eccentricity of 0.4 in direction 45^{o} to the horizontal and Rayleigh number of 10, 80 and 120 respectively

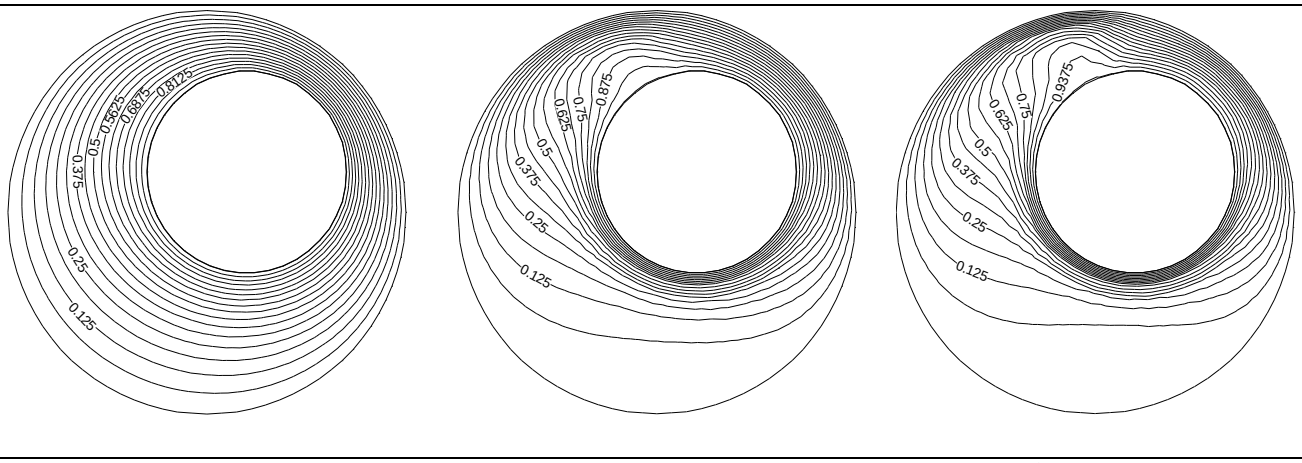

Fig. (21) Isotherms contours for relative eccentricity of 0.4 in direction 45^{o} to the horizontal and Rayleigh number of 10, 80 and 120 respectively

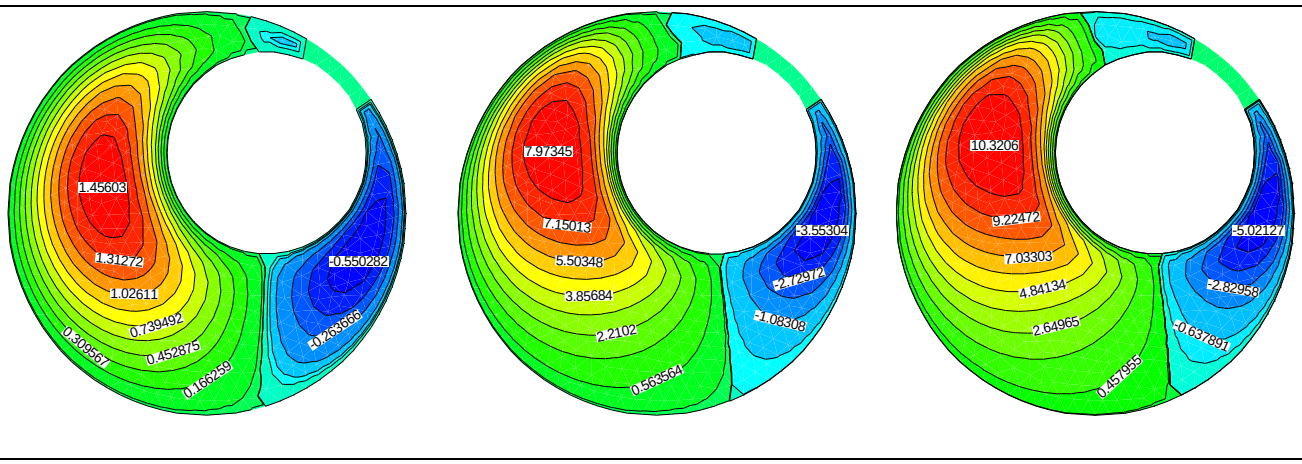

Fig. (22) Isotherms contours for relative eccentricity of 0.6 in direction 45^{o} to the horizontal and Rayleigh number of 10, 80 and 120 respectively

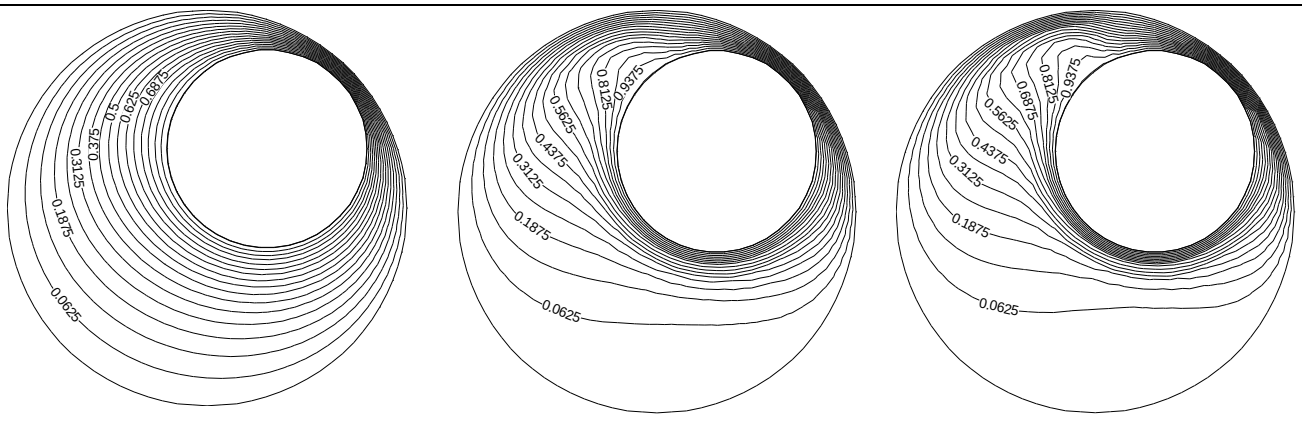

Fig. (23) Isotherms contours for relative eccentricity of 0.6 in direction 45^{o} to the horizontal and Rayleigh number of 10, 80 and 120 respectively

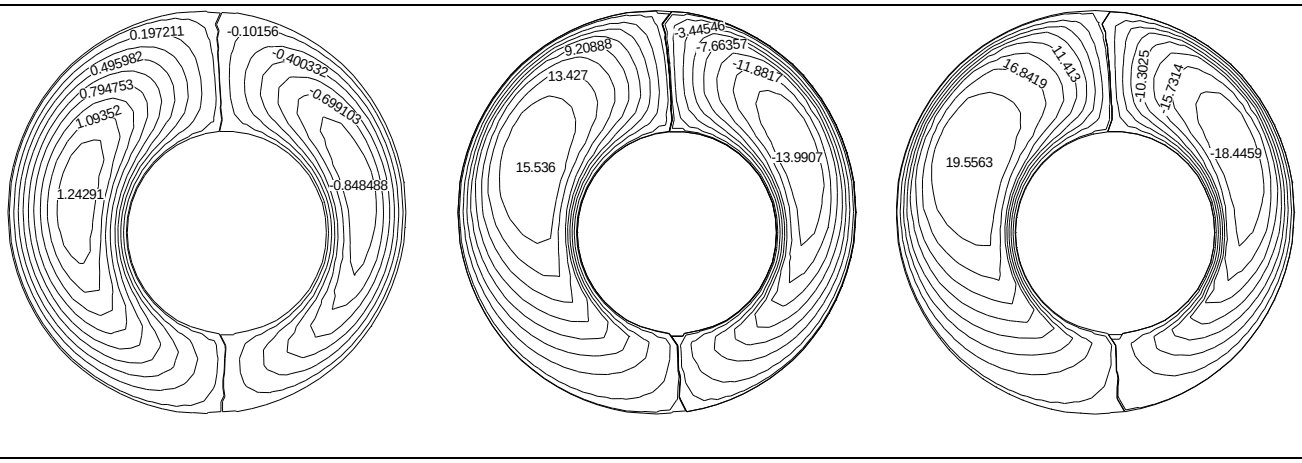

Fig. (24) Stream function contours for relative eccentricity of 0.2 in direction 315^{o} to the horizontal and Rayleigh number of 10, 200 and 300 respectively

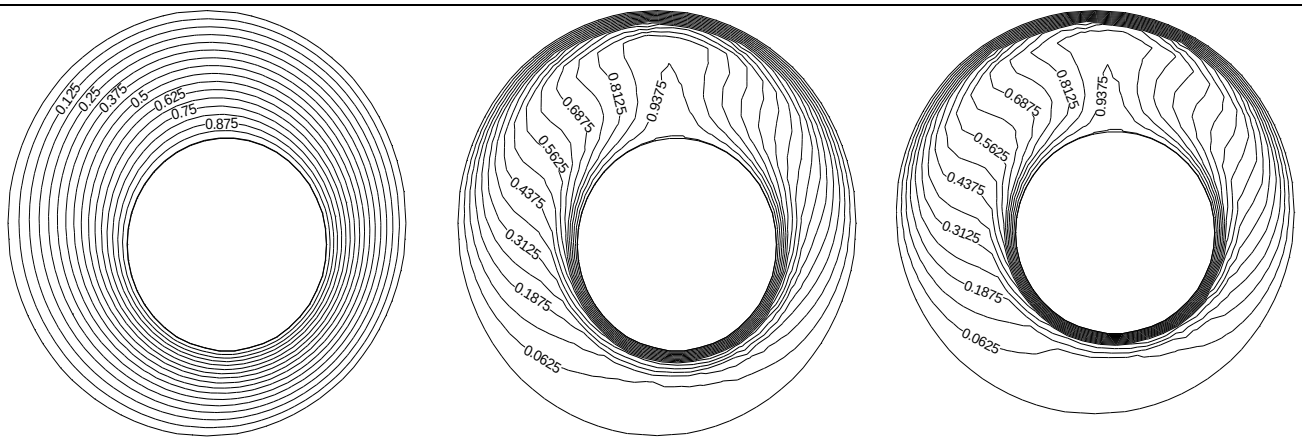

Fig. (25) Isotherms contours for relative eccentricity of 0.2 in direction 315^{o} to the horizontal and Rayleigh number of 10, 200 and 300 respectively

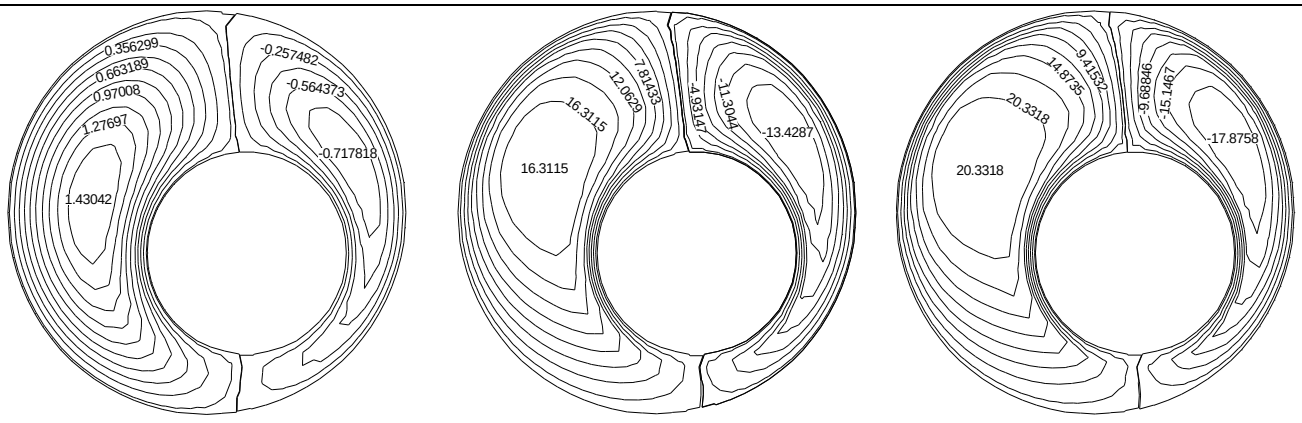

Fig. (26) Stream function contours for relative eccentricity of 0.4 in direction 315^{o} to the horizontal and Rayleigh number of 10, 200 and 300 respectively

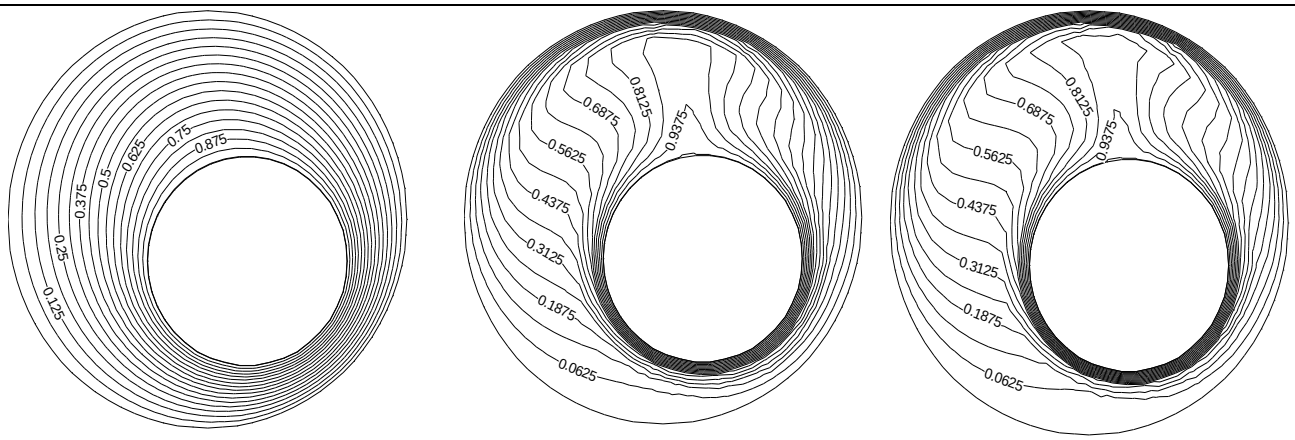

Fig. (27) Isotherms contours for relative eccentricity of 0.4 in direction 315^{o} to the horizontal and Rayleigh number of 10, 200 and 300 respectively

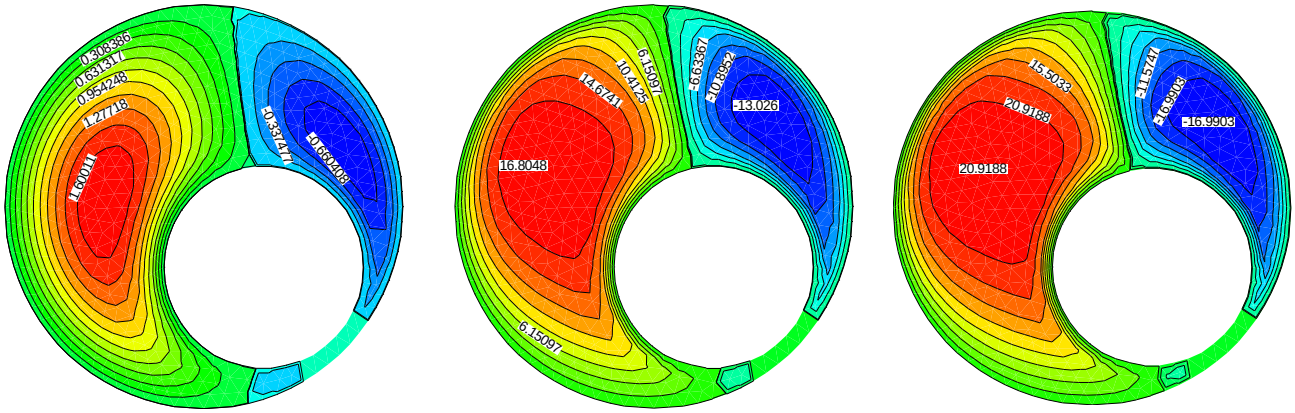

Fig. (28) Stream function contours for relative eccentricity of 0.6 in direction 315^{o} to the horizontal and Rayleigh number of 10, 200 and 300 respectively

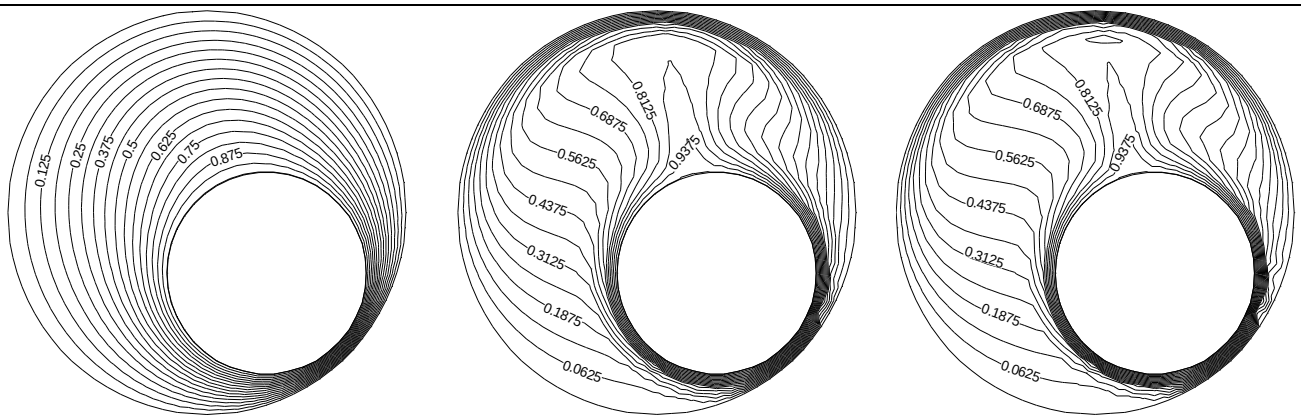

Fig. (29) Isotherms contours for relative eccentricity of 0.6 in direction 315^{o} to the horizontal and Rayleigh number of 10, 200 and 300 respectively